East European Journal of Physics. 1. 447-459 (2026)
DOI:10.26565/2312-4334-2026-1-52 ISSN 2312-4334

FINITE DIFFERENCE ANALYSIS OF PRANDTL NUMBER AND PARTICLE VOLUME FRACTION EFFECTS ON SKIN FRICTION AND HEAT TRANSFER IN BUOYANCY DRIVEN TWO-PHASE FLOW WITH SUSPENDED PARTICULATE MATTER (SPM)

Sasanka Sekhar Bishoyi[1], Sakambari Mishra[2], Aditya Kumar Pati[3]*, Prasanta Kumar Rath[3]
[1]*NIST University, Berhampur, Ganjam, Odisha, India*
[2]*College of Basic Science and Humanities, Odisha University of Agriculture and Technology, Bhubaneswar, Odisha, India*
[3]*Centurion University of Technology and Management, Paralakhemundi, Odisha, India*
**Corresponding author e-mail: apati@cutm.ac.in*
Received December 2, 2025; revised January 15, 2026; accepted January 20, 2026

A numerical investigation has been conducted on incompressible, laminar two-phase buoyancy driven flow containing suspended particles around a vertical plate. Despite the relevance of such systems, prior studies have largely overlooked natural convection two-phase flows with particulate matter, particularly concerning the roles of parameters like the Prandtl number and volume fraction. Addressing this research gap is crucial, as these parameters significantly influence flow behavior and heat transfer, which are vital in environmental, industrial, and thermal applications. This study focuses on exploring the effects of volume fraction and Prandtl number on two-phase flow characteristics using an implicit finite difference method applied on a non-uniform grid. The analysis evaluates boundary layer behavior, heat transfer rates, and skin friction coefficients. Streamline patterns are illustrated for different Prandtl number values, while contour topologies are presented to demonstrate the combined influence of the Prandtl number and volume fraction on skin friction and the heat transfer rate. Results show that increasing the volume fraction reduces both the Nusselt number and the skin friction coefficient, while a higher Prandtl number enhances both. The enhanced thermal response observed with higher Prandtl numbers is particularly beneficial in manufacturing processes involving flat wall-like structures that are susceptible to thermal stress. These findings hold practical significance for the design and optimization of heat exchangers, lubrication systems, and thermal management solutions in electronic devices.

Keywords: *Heat Transfer; Buoyancy driven flow; Prandtl Number; Particle Volume Fraction; Suspended Particulate Matter; Implicit Finite Difference Method*

PACS: 44.05.+e, 44.20.+b, 44.25.+f, 47.10.ad, 47.11.Bc, 47.15.Cb

1. INTRODUCTION

Natural convection is an essential heat transfer process occurring in fluids, primarily driven by buoyancy forces that arise due to differences in temperature. This phenomenon significantly influences a broad spectrum of uses, from environmental processes such as ocean currents and atmospheric circulation to various industrial systems like cooling mechanisms in power plants and electronic devices. The ability of natural convection to efficiently transfer heat without requiring external mechanical forces makes it a key factor in maintaining thermal equilibrium and enhancing the performance of both natural and engineered systems. Many natural convection processes take place in environments characterized by temperature stratification. For example, a room warmed by electric wires installed in the ceiling can develop thermal stratification. Similarly, in the case of a fire in a room with an open door or window, fresh air flows in near the floor, resulting in a layered thermal effect. Accurately predicting heat transfer in natural convective flows is crucial for various engineering applications, including building climate control, electronics cooling, heat exchange processes, and safety considerations such as managing heat from fires. The analysis of natural convective flow past a vertical plate has been extensively researched because of its wide-ranging applications in engineering, such as building climate management, cooling electronic devices, and the growth of crystals. It remains a significant topic of interest both theoretically and experimentally because of the numerous potential variations in boundary conditions. Several studies [1-7] have focused on investigating natural convection past a vertical plate within a stratified medium, recognizing its significant importance. Recently, several researchers have focused on two-phase flow in the context of heat transfer applications. For instance, Obalalu et al. [8] investigated the influence of a heat source/sink and solar radiation on two-phase flow over a vertically deformable sheet. Hameed et al. [9] examined natural convection and heat transfer in dome-shaped enclosures filled with nanofluids under two-phase flow conditions. Shi et al. [10] conducted an experimental study on two-phase flow instability triggered by direct contact condensation in an open natural circulation system. Akter et al. [11] carried out a finite difference simulation to analyze natural convection in two-phase flow along a vertically heated wavy surface. More recently, Zamri et al. [12] studied the impact of fluid-particle interaction and mass concentration on velocity, temperature, and skin friction in two-phase flow. Earlier research focused on finding similarity solutions, as these variables provide substantial physical insights with minimal effort. The diversity in approaches highlights the complex nature of these thermal processes and the ongoing need to understand them better.

Cite as: S.S. Bishoyi, S. Mishra, A.K. Pati, P.K. Rath, East Eur. J. Phys. 1, 447 (2026), https://doi.org/10.26565/2312-4334-2026-1-52

Dust particles in the boundary layer can originate from various sources, such as combustion processes, flow dynamics in rocket tubes, dust entrainment in clouds during nuclear explosions, soil erosion due to natural winds, blood flow in capillaries and paint spraying. A comprehensive understanding of particle interactions with fluid flows is crucial in each of these situations. Understanding this knowledge is essential for efficiently applying computational fluid dynamics (CFD) models to improve and optimize the effectiveness of current machinery and procedures, identify and resolve operational issues, explore retrofit possibilities, and design new systems and plants, including scaling up processes. To address these needs, numerous researchers have developed and thoroughly examined multiphase flow equations to better predict and control such complex interactions. Soo [13] has created a mathematical framework for exploring multiphase flows. In recent years, a number of studies [14-30] have focused on examining two-phase flow or boundary layer flow, highlighting the increasing interest in these phenomena due to their significant implications for practical heat transfer applications. Researchers have been exploring how these flow dynamics impact various thermal processes, demonstrating their relevance in improving the efficiency and effectiveness of heat transfer systems.

Earlier investigations on natural convection have largely focused on single-phase fluids, with relatively limited emphasis on flows involving suspended particulate matter (SPM). In particular, the existing literature highlights a clear deficiency in studies addressing the coupled influence of particle volume fraction and Prandtl number in two-phase natural convection flows involving suspended particulate matter. Although natural convective boundary layer flow over a vertical plate plays a vital role in many engineering and environmental applications including industrial cooling, heat exchanger design, and pollutant dispersion, the effects of suspended particulates on such flows have not been adequately quantified. Most reported studies either neglect particulate effects or treat them in a simplified manner, thereby overlooking their significant impact on momentum and thermal transport mechanisms.

This research gap is critical because the presence of suspended particles can substantially modify both the momentum boundary layer and the thermal boundary layer through complex particle–fluid interactions, leading to notable variations in skin friction and heat transfer rates. Furthermore, changes in particle concentration (volume fraction) directly influence the effective thermophysical properties of the fluid, while variations in the Prandtl number govern the relative dominance of momentum diffusivity and thermal diffusivity. Despite their practical importance, the combined and interactive effects of these parameters on skin friction and heat transfer characteristics in two-phase natural convection flows involving suspended particulate matter remain insufficiently explored.

Motivated by this unresolved gap, the present investigation offers a novel and systematic analysis of the simultaneous effects of Prandtl number and volume fraction on boundary layer characteristics, heat transfer, and skin friction in steady, laminar, incompressible two-phase natural convective flow along a vertical plate containing suspended particulates. By employing a reliable finite difference numerical technique, this study provides new physical insights into particulate-laden natural convection and contributes to the advancement of accurate modeling and efficient thermal system design involving two-phase convective flows.

2. MATHEMATICAL ANALYSIS

To demonstrate the effects of Prandtl number and volume fraction, we examined a plate that is extensive in both length and width, positioned in a plane that is vertical to the floor, and has the capacity to be either heated or cooled. The x-coordinate is oriented along the plate, while the y-coordinate is oriented perpendicular to it. The temperature of the plate surface is denoted as T_w, and it asymptotically reduces to the ambient fluid temperature T_∞ as one move away from the plate. The fluid velocity at the plate surface starts from zero, increases to a maximum near the surface, and then asymptotically decreases to zero at greater distances. The temperature and velocity of the particle phase differ from those of the fluid on the plate. Figure 1 illustrates the geometry of the flow.

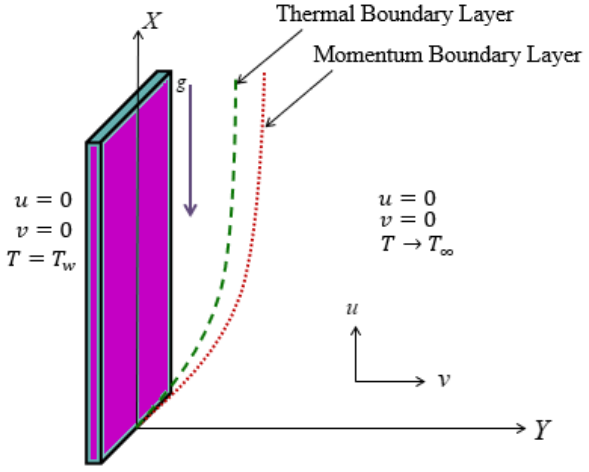

Figure 1. Geometry of the flow

Otterman [31] showed that traditional boundary layer approximations can be applied to the fluid phase when the particulate phase density is similar to that of the fluid. Additionally, it has been established that the boundary layer approximation is not needed for the momentum equations governing the particle phase, and it is essential to account for the transverse component of particle momentum. Consequently, in this context, the y-component of the momentum equation for the fluid phase is omitted, while the particle phase y-component is maintained.

Based on the assumptions outlined earlier, the governing equations describing the two-phase flow, as formulated by Tripathy et al. [14], Mishra et al. [15] and Misra et al. [32], are given below:

$$\frac{\partial u}{\partial x}+\frac{\partial v}{\partial y}=0 \tag{1}$$

$$u_p\frac{\partial \rho_p}{\partial x}+v_p\frac{\partial \rho_p}{\partial y}=D_p\frac{\partial^2 \rho_p}{\partial y^2} \tag{2}$$

$$(1-\varphi)\rho\left(u\frac{\partial u}{\partial x}+v\frac{\partial u}{\partial y}\right)=(1-\varphi)\mu\frac{\partial^2 u}{\partial y^2}-\frac{1}{\tau_p}\varphi\rho_s(u-u_p)+(1-\varphi)\rho g\beta(T-T_\infty) \tag{3}$$

$$\varphi\rho_s\left(u_p\frac{\partial u_p}{\partial x}+v_p\frac{\partial u_p}{\partial y}\right)=\frac{\partial}{\partial y}\left(\varphi\mu_s\frac{\partial u_p}{\partial y}\right)+\frac{1}{\tau_p}\varphi\rho_s(u-u_p)+\varphi(\rho_s-\rho)g \tag{4}$$

$$\varphi\rho_s\left(u_p\frac{\partial v_p}{\partial x}+v_p\frac{\partial v_p}{\partial y}\right)=\frac{\partial}{\partial y}\left(\varphi\mu_s\frac{\partial v_p}{\partial y}\right)+\frac{1}{\tau_p}\varphi\rho_s(v-v_p) \tag{5}$$

$$(1-\varphi)\rho c_p\left(u\frac{\partial T}{\partial x}+v\frac{\partial T}{\partial y}\right)=(1-\varphi)\,k\frac{\partial^2 T}{\partial y^2}+\frac{1}{\tau_T}\varphi\rho_s c_s(T_p-T)+(1-\varphi)\mu\left(\frac{\partial u}{\partial y}\right)^2 \tag{6}$$

$$\varphi\,\rho_s c_s\left(u_p\frac{\partial T_p}{\partial x}+v_p\frac{\partial T_p}{\partial y}\right)=\frac{\partial}{\partial y}\left(\varphi k_s\frac{\partial T_p}{\partial y}\right)-\frac{1}{\tau_T}\varphi\rho_s c_s(T_p-T)+\varphi\mu_s\left[u_p\frac{\partial^2 u_p}{\partial y^2}+\left(\frac{\partial u_p}{\partial y}\right)^2\right] \tag{7}$$

Here D_p is the binary diffusion coefficient. If the variation of temperature is minimal; D_p, μ_s and k_s can be assumed to be constant. In this case, the term $\frac{\partial}{\partial y}\left(\varphi\mu_s\frac{\partial u_p}{\partial y}\right)$ can be replaced by $\varphi\mu_s\frac{\partial^2 u_p}{\partial y^2}$, in the particle phase x-momentum equation, reflecting the random motion of particles, analogous to similar terms in the fluid phase. Additionally, the term $\frac{\partial}{\partial y}\left(\varphi k_s\frac{\partial T_p}{\partial y}\right)$ in the energy equation for particle phase may be substituted with $\varphi k_s\frac{\partial^2 T_p}{\partial y^2}$. Generally, $D_p\approx\upsilon_p$ and D_p is often significantly smaller than υ. Nevertheless, we choose to retain the terms involving D_p and υ_p to examine their respective impacts on the solutions of these equations, regardless of how minimal these influences may be in many flow scenarios.

Given the above considerations, equations (1) through (7) simplify to

$$\frac{\partial u}{\partial x}+\frac{\partial v}{\partial y}=0 \tag{8}$$

$$v_p\frac{\partial \rho_p}{\partial y}+u_p\frac{\partial \rho_p}{\partial x}=\upsilon_p\frac{\partial^2 \rho_p}{\partial y^2} \tag{9}$$

$$v\frac{\partial u}{\partial y}+u\frac{\partial u}{\partial x}=\nu\frac{\partial^2 u}{\partial y^2}+g\beta(T-T_\infty)-(u-u_p)\frac{1}{1-\varphi}\,\frac{1}{\tau_p}\frac{\rho_p}{\rho} \tag{10}$$

$$v_p\frac{\partial u_p}{\partial y}+u_p\frac{\partial u_p}{\partial x}=\nu_s\frac{\partial^2 u_p}{\partial y^2}+\left(1-\frac{\rho}{\rho_s}\right)g+\frac{1}{\tau_p}(u-u_p) \tag{11}$$

$$v_p\frac{\partial v_p}{\partial y}+u_p\frac{\partial v_p}{\partial x}=-\frac{1}{\tau_p}(v_p-v)+\nu_s\frac{\partial^2 v_p}{\partial y^2} \tag{12}$$

$$v\frac{\partial T}{\partial y}+u\frac{\partial T}{\partial x}=\frac{1}{1-\varphi}\frac{1}{\tau_T}(T_p-T)\frac{\rho_p}{\rho}\frac{C_s}{C_p}+\frac{\mu}{\rho C_p}\left(\frac{\partial u}{\partial y}\right)^2+\frac{\kappa}{\rho C_p}\frac{\partial^2 T}{\partial y^2} \tag{13}$$

$$v_p\frac{\partial T_p}{\partial y}+u_p\frac{\partial T_p}{\partial x}=\frac{\mu_s}{\rho_s C_s}\left[u_p\frac{\partial^2 u_p}{\partial y^2}+\left(\frac{\partial u_p}{\partial y}\right)^2\right]-\frac{1}{\tau_T}(T_p-T)+\frac{\kappa_s}{\rho_s C_s}\frac{\partial^2 T_p}{\partial y^2} \tag{14}$$

Introducing the dimensionless variables such as

$y^*=\frac{y}{L}\sqrt{Re}$, $x^*=\frac{x}{L}$, $v^*=\frac{v}{U}\sqrt{Re}$, $u^*=\frac{u}{U}$, $v_p^*=\frac{v_p}{U}\sqrt{Re}$, $u_p^*=\frac{u_p}{U}$, $T_p{}^*=\frac{T_p-T_\infty}{T_w-T_\infty}$, $T^*=\frac{T-T_\infty}{T_w-T_\infty}$, $\rho_p^*=\frac{\rho_p}{\rho_{p_0}}$, $\rho_s^*=\frac{\rho_s}{\rho_{p_0}}$,

in the equations numbered (8) through (14), and after omitting the asterisks, the fundamental boundary layer equations describing the flow field, as outlined by Tripathy et al. [14], are given by

$$\frac{\partial u}{\partial x}=-\frac{\partial v}{\partial y} \tag{15}$$

$$v_p\frac{\partial \rho_p}{\partial y}+u_p\frac{\partial \rho_p}{\partial x}=\epsilon\frac{\partial^2 \rho_p}{\partial y^2} \tag{16}$$

$$v\,\frac{\partial u}{\partial y}+u\,\frac{\partial u}{\partial x}=\frac{Gr\,T}{Re^2}-\alpha\rho_p(u-u_p)\frac{1}{1-\varphi}\,\frac{F\,L}{U}+\frac{\partial^2 u}{\partial y^2} \tag{17}$$

$$u_p\frac{\partial u_p}{\partial x}+v_p\frac{\partial u_p}{\partial y}=\frac{1}{Fr}\left(1-\frac{1}{\gamma}\right)+\frac{F\,L}{U}(u-u_p)+\epsilon\,\frac{\partial^2 u_p}{\partial y^2} \tag{18}$$

$$v_p\frac{\partial v_p}{\partial y}+u_p\frac{\partial v_p}{\partial x}=\frac{F\,L}{U}(v-v_p)+\epsilon\,\frac{\partial^2 v_p}{\partial y^2} \tag{19}$$

$$v\frac{\partial T}{\partial y}+u\frac{\partial T}{\partial x}=\frac{1}{Pr}\,\frac{\partial^2 T}{\partial y^2}+\frac{2\,\alpha}{3\,Pr}\frac{F\,L}{U}\rho_p(T_p-T)\,\frac{1}{1-\varphi}+Ec\left(\frac{\partial u}{\partial y}\right)^2 \tag{20}$$

$$v_p\frac{\partial T_p}{\partial \eta}+u_p\frac{\partial T_p}{\partial x}=\frac{F\,L}{U}\,(T-T_p)+\frac{3}{2}Pr\,\epsilon Ec\left[\left(\frac{\partial u_p}{\partial y}\right)^2+u_p\,\frac{\partial^2 u_p}{\partial y^2}\right]+\frac{\epsilon}{Pr}\,\frac{\partial^2 T_p}{\partial y^2}, \tag{21}$$

with the boundary conditions (Misra et al. [32])

$$y=0:\rho_p=\rho_{pw}(x),T_p=T_{pw}(x),T=T_w=1,v=0,u=0\,,v_p=0,u_p=u_{pw}(x), \tag{22}$$

$$y\to\infty:,\ \rho_p=1,T_p=0,T=T_\infty=0,v_p=0,u=u_p=0. \tag{23}$$

Computational algorithm of the present study is depicted in Fig. 2.

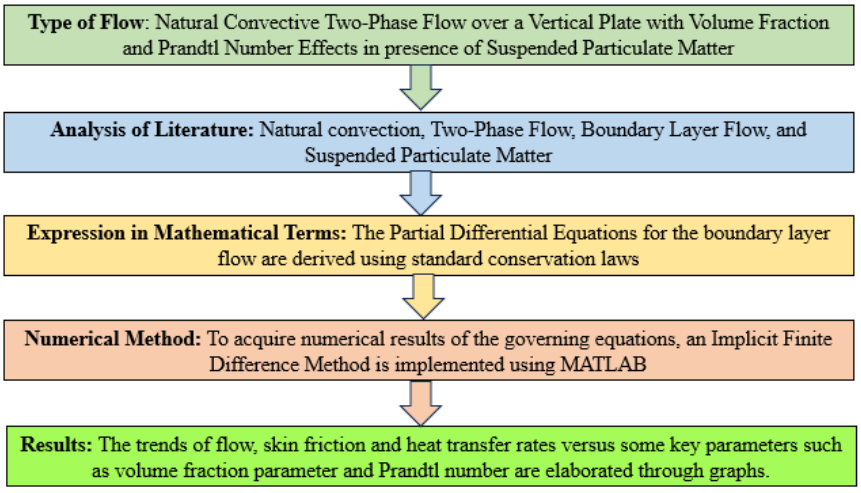

Figure 2. Computational algorithm

3. METHOD OF SOLUTION:

Finite difference expressions are utilized for the different terms in equations (15) to (21) as follows in order to create a computational procedure that makes use of a non-uniform grid:

$$\frac{\partial W}{\partial x}=\frac{0.5\,W_j^{n-1}-2W_j^n+1.5\,W_j^{n+1}}{\Delta x}+o(\Delta x^2) \tag{24}$$

$$\frac{\partial W}{\partial y}=\frac{W_{j+1}^{n+1}-r_y^2\,W_{j-1}^{n+1}-(1-r_y^2)W_j^{n+1}}{r_y\,(r_y+1)\,\Delta y}+o(\Delta y^2) \tag{25}$$

$$\frac{\partial^2 W}{\partial y^2}=2\,\frac{r_y\,W_{j-1}^{n+1}-(1+r_y)W_j^{n+1}+W_{j+1}^{n+1}}{(r_y+1)r_y\,\Delta y^2}+o(\Delta y^2) \tag{26}$$

$$W_j^{n+1}=-W_j^{n-1}+2\,W_j^n+o(\Delta x^2) \tag{27}$$

and

$$y_{j+1}-y_j=-(y_{j-1}-y_j)r_y=r_y\Delta y_j \tag{28}$$

where W can represent either T or T_p or u or u_p or $v_p$or v or ρ_p.

A typical three-point representation of $\frac{\partial W}{\partial y}$ on a non-uniform grid is employed here to achieve the minimal truncation error.

Equations (15) through (21) are transformed into difference equations in accordance with the methodology proposed by Mishra and Tripathy [33] as follows:

$$v_j^{n+1}=-\frac{1}{2}\frac{\Delta y}{\Delta x}\left[\left(0.5\,u_j^{n-1}-2\,u_j^n+1.5\,u_j^{n+1}\right)+\left(0.5\,u_{j-1}^{n-1}-2\,u_{j-1}^n+1.5\,u_{j-1}^{n+1}\right)\right]+v_{j-1}^{n+1} \tag{29}$$

$$a_j u_{j-1}^{n+1}=d_j-b_j u_j^{n+1}-c_j u_{j+1}^{n+1} \tag{30}$$

$$a_j^* u_{p_{j-1}}^{n+1} = d_j^* - b_j^* u_{p_j}^{n+1} - c_j^* u_{p_{j+1}}^{n+1} \tag{31}$$

$$a_j^{**} v_{p_{j-1}}^{n+1} = d_j^{**} - b_j^{**} v_{p_j}^{n+1} - c_j^{**} v_{p_{j+1}}^{n+1} \tag{32}$$

$$a_j^{+} T_{j-1}^{n+1} = d_j^{+} - b_j^{+} T_j^{n+1} - c_j^{+} T_{j+1}^{n+1} \tag{33}$$

$$a_j^{++} T_{p_{j-1}}^{n+1} = d_j^{++} - b_j^{++} T_{p_j}^{n+1} - c_j^{++} T_{p_{j+1}}^{n+1} \tag{34}$$

$$a_j^{\blacksquare} \rho_{p_{j-1}}^{n+1} = d_j^{\blacksquare} - b_j^{\blacksquare} \rho_{p_j}^{n+1} \; c_j^{\blacksquare} \rho_{p_{j+1}}^{n+1} \tag{35}$$

Where:

$$a_j = \frac{1}{\Delta x}\left[-q - p r_y\right] \tag{36}$$

$$b_j = \frac{1}{\Delta x}\left[p\left(r_y - \frac{1}{r_y}\right) + 1.5\ \left(2\,u_j^n - u_j^{n-1}\right) + \frac{1}{1-\varphi}\frac{FL}{U}\alpha\Delta x\left(2\,\rho_{p_j}^{\,n} - \rho_{p_j}^{\,n-1}\right) + q\left(1 + \frac{1}{r_y}\right)\right] \tag{37}$$

$$c_j = \frac{1}{\Delta x}\left[\frac{1}{r_y}(p-q)\right] \tag{38}$$

$$d_j = \frac{1}{\Delta x}\begin{bmatrix} \frac{Gr\left(2T_j^n - T_j^{n-1}\right)}{Re^2}\Delta x + \left(-u_j^{n-1} + 2\,u_j^n\right)\left(-0.5\,u_j^{n-1} + 2\,u_j^n\right) \\ -\frac{\varphi}{1-\varphi}\frac{FL}{U}\,\alpha\left(2\,\rho_{p_j}^{\,n} - \rho_{p_j}^{\,n-1}\right)\left(-\,2\,u_{p_j}^{\,n} + \,u_{p_j}^{\,n-1}\right)\Delta x \end{bmatrix} \tag{39}$$

$$a_j^* = \frac{1}{\Delta x}\left[-\epsilon q - p r_y\right] \tag{40}$$

$$b_j^* = \frac{1}{\Delta x}\left[1.5\ \left(2\,u_{p_j}^{\,n} - u_{p_j}^{\,n-1}\right) + \epsilon q\left(1 + \frac{1}{r_y}\right) + \frac{FL}{U}\,\Delta x + \,p\left(r_y - \frac{1}{r_y}\right)\right] \tag{41}$$

$$c_j^* = \frac{1}{\Delta x}\left[\frac{1}{r_y}(-\epsilon q + p)\right] \tag{42}$$

$$d_j^* = \frac{1}{\Delta x}\left[\left(2\,u_{p_j}^{\,n} - \,u_{p_j}^{\,n-1}\right)\left(2\,u_{p_j}^{\,n} - \,0.5\,u_{p_j}^{\,n-1}\right) + \frac{1}{Fr}\left(1 - \frac{1}{\gamma}\right)\Delta x + \frac{FL}{U}\,\Delta x\,u_j^{n+1}\right] \tag{43}$$

$$a_j^{**} = \frac{1}{\Delta x}\left[-\epsilon q - p r_y\right] \tag{44}$$

$$b_j^{**} = \frac{1}{\Delta x}\left[\frac{FL}{U}\,\Delta x + 1.5\ u_{p_j}^{\,n+1} + \,\epsilon q\left(1 + \frac{1}{r_y}\right) + \,p\left(r_y - \frac{1}{r_y}\right)\right] \tag{45}$$

$$c_j^{**} = \frac{1}{\Delta x}\left[\frac{1}{r_y}(-\epsilon q + p)\right] \tag{46}$$

$$d_j^{**} = \frac{1}{\Delta x}\left[\frac{FL}{U}\,\Delta x\,v_j^{n+1} + u_{p_j}^{\,n+1}\left(2\,v_{p_j}^{\,n} - 0.5\,v_{p_j}^{\,n-1}\right)\right] \tag{47}$$

$$a_j^{+} = \frac{1}{\Delta x}\left[-q\left(\frac{1}{Pr} + 0.5\,r_y\,\Delta y\,v_j^{n+1}\right)\right] \tag{48}$$

$$b_j^{+} = \frac{1}{\Delta x}\left[0.5\,q\,\Delta y\,v_j^{n+1}\left(r_y - \frac{1}{r_y}\right) + 1.5\,u_j^{n+1} + \frac{2\alpha}{3\,Pr}\,\frac{1}{1-\varphi}\,\frac{FL}{U}\,\Delta x\,\rho_{p_j}^{\,n+1} + \frac{q\,(1+r_y)}{Pr.r_y}\right] \tag{49}$$

$$c_j^{+} = \frac{1}{\Delta x}\left[\frac{q}{r_y}\left(-\frac{1}{Pr} + 0.5\,\Delta y\,v_j^{n+1}\right)\right] \tag{50}$$

$$d_j^{+} = \frac{1}{\Delta x}\begin{bmatrix} \frac{2\alpha}{3\,Pr}\,\frac{1}{1-\varphi}\,\frac{FL}{U}\,\rho_{p_j}^{\,n+1}\left(2\,T_{p_j}^{\,n} - \,T_{p_j}^{\,n-1}\right)\Delta x \\ +u_j^{n+1}\left(2\,T_j^n - 0.5\,T_j^{n-1}\right) + \Delta x.\,Ec\left(\frac{u_{j+1}^{n+1} - u_j^{n+1}}{\Delta y}\right)^2 \end{bmatrix} \tag{51}$$

$$a_j^{++} = \frac{1}{\Delta x}\left[\frac{\epsilon}{Pr} - q\left(\frac{1}{2}\,\Delta y\,r_y\,v_{p_j}^{\,n+1}\right)\right] \tag{52}$$

$$b_j^{++} = \frac{1}{\Delta x}\left[\,1.5\,u_{p_j}^{\,n+1} + \frac{\epsilon\,q\,(1+r_y)}{Pr.r_y} + \,\frac{FL}{U}\,\Delta x\, + 0.5\,q\,\Delta y\,v_{p_j}^{\,n+1}\left(r_y - \frac{1}{r_y}\right)\right] \tag{53}$$

$$c_j^{++} = \frac{1}{\Delta x}\left[\frac{q}{r_y}\left(-\frac{\epsilon}{Pr} + 0.5\Delta y.\,v_{p_j}^{\,n+1}\right)\right] \tag{54}$$

$$d_j^{++} = \frac{1}{\Delta x}\left[\begin{array}{c}\frac{FL}{U}\ T_j^{n+1}\Delta x + u_{p_j}^{n+1}\left(2\,T_{p_j}^{\,n} - 0.5\,T_{p_j}^{\,n-1}\right)\\ +\frac{3}{2}Pr.\epsilon.Ec.\Delta x\left\{\left(\frac{u_{p_{j+1}}^{n+1} - u_{p_j}^{n+1}}{\Delta y}\right)^2 + 2u_{p_j}^{\,n+1}\left(\frac{u_{p_{j-1}}^{n+1} - \left(1+\frac{1}{r_y}\right)u_{p_j}^{n+1} + \frac{1}{r_y}u_{p_{j+1}}^{n+1}}{(1+r_y)\ \Delta y^2}\right)\right\}\end{array}\right] \quad (55)$$

$$a_j^{\blacksquare} = -2\epsilon\, r_y\ -\ v_{p_j}^{\,n+1} r_y^2\,\Delta y \quad (56)$$

$$b_j^{\blacksquare} = 2\epsilon\left(1 + r_y\right) -\ v_{p_j}^{\,n+1}\left(1 - r_y^2\right)\Delta y + \frac{1.5\,p^{\blacksquare}\,u_{p_j}^{\,n+1}}{\Delta x} \quad (57)$$

$$c_j^{\blacksquare} = -2\epsilon + p^{\blacksquare}\,v_{p_j}^{\,n+1}\Delta y \quad (58)$$

$$d_j^{\blacksquare} = p^{\blacksquare}\,u_{p_j}^{\,n+1}\frac{-\,0.5\,\rho_{p_j}^{\,n-1} + 2\rho_{p_j}^{\,n}}{\Delta x} \quad (59)$$

$$p = \left(2\,v_j^n -\ v_j^{n-1}\right)\frac{\Delta x}{(1+r_y)\Delta y} \quad (60)$$

$$q = \frac{2\,\Delta x}{\left(1 +\ r_y\right)\Delta y^2}$$

$$p^{\blacksquare} = r_y\left(r_y + 1\right)\Delta y^2 \quad (61)$$

The equations (30) to (35) cannot be applied at $j = 1$ or $j = jmax$ due to the boundary conditions (22) and (23). Therefore,

$a_2 = 0$ as $u_1 = 0$ at $j = 2$
$c_j = 0$ at $j = j_{max} - 1$
$d_2^* = d_2^* - a_2^* v_{pw}$ at $j = 2$
$c_j^* = 0$ at $j = j_{max} - 1$
$a_2^{**} = 0$ at $j = 2$
$c_j^{**} = 0$ at $j = j_{max} - 1$
$d_2^+ = d_2^+ - a_2^+$ at $j = 2$
$c_j^+ = 0$ at $j = j_{max} - 1$
$d_2^{++} = d_2^{++} - a_2^{++} T_{pw}$ at $j = 2$
$c_j^{++} = 0$ at $j = j_{max} - 1$
$d_2^{\blacksquare} = d_2^{\blacksquare} - a_2^{\blacksquare}\rho_{pw}$ at $j = 2$
$d_j^{\blacksquare} = d_j^{\blacksquare} - c_j^{\blacksquare}$ at $j = j_{max} - 1$

Computation of u_{pw} at $y = 0$:
Since u_{pw} depends solely on x, we can derive from equation (18) that

$$u_{p1}^{n+1} = +\frac{2}{3}\frac{\Delta x}{Fr}\left(1 - \frac{1}{\gamma}\right) + \frac{4}{3}u_{p1}^n - \frac{1}{3}u_{p1}^{n-1} - \frac{2}{3}\frac{FL}{U}\Delta x \quad (62)$$

Computation of T_{pw} at y= 0:
As T_{pw} depends solely on x, we can derive from equation (18) that

$$T_{p_1}^{\,n+1} = \frac{\frac{FL}{U}\frac{\Delta x}{u_{p_1}^{n+1}} + 2T_{p_1}^{\,n} - 0.5T_{p_1}^{\,n-1}}{1.5 + \frac{FL}{U}\frac{\Delta x}{u_{p_1}^{n+1}}} \quad (63)$$

Heat transfer:
The Nusselt number, defined as follows, represents the qualities of heat transfer:

$$Nu^{\,n+1} = -\sqrt{Re}\left[\frac{\partial T}{\partial y}\right]_{y=0}^{n+1} = -\sqrt{Re}\left[\frac{T_{j+1}^{n+1} - r_y^2 T_{j-1}^{n+1} - \left(1 - r_y^2\right)T_j^{n+1}}{r_y(1+r_y)\Delta y}\right]_{j=2} = -\sqrt{Re}\left[\frac{-r_y^2 T_1^{n+1} + T_3^{n+1} - \left(1 - r_y^2\right)T_2^{n+1}}{r_y(r_y+1)\Delta y}\right] \quad (64)$$

Computation of skin friction coefficient:

$$C_f = \frac{\tau_w}{0.5\rho U^2} = \frac{2}{U^2\sqrt{Re}}\left.\frac{\partial u}{\partial y}\right]_{y=0}$$

Through the application of finite differences, the equation above simplifies to

$$C_f^{n+1} = \frac{2}{U^2\sqrt{Re}}\left[\frac{u_{j+1}^{n+1} - r_y^2 u_{j-1}^{n+1} - (1-r_y^2)u_j^{n+1}}{r_y(1+r_y)\Delta y}\right]_{j=2} = \frac{2}{U^2\sqrt{Re}}\left[\frac{u_3^{n+1} - r_y^2 u_1^{n+1} - (1-r_y^2)u_2^{n+1}}{r_y(1+r_y)\Delta y}\right] \quad (65)$$

Figure 3 illustrates the grid independence analysis, demonstrating the convergence of the Nusselt number as the number of grid points increases. A grid independence test was performed using grid sizes ranging from 20 to 192 points. The Nusselt number exhibits monotonic convergence, and variations beyond 190 grid points are negligible. Hence, a grid size of 192 points was selected for all subsequent computations.

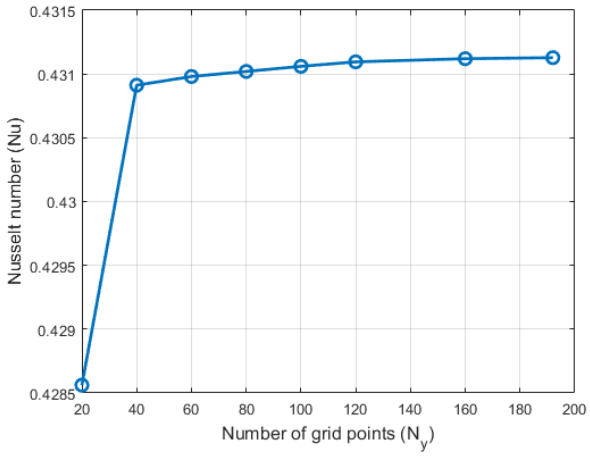

Figure 3. Grid independence study showing convergence of the Nusselt number with increasing number of grid points

4. DISCUSSION OF THE RESULTS

This study examines the essential characteristics of two-phase momentum and thermal boundary layer flow across a semi-infinite flat plate, using the finite difference method for its analysis.

We chose the subsequent values for the different parameters involved.

$\varphi = 0.01, 0.05, 0.1$; $Pr = 0.71, 1.0, 7.0$; $U = 0.45\ m/sec$; $\epsilon = 0.1$;

$\rho = 0.913\ \ kg/m^3$; $\rho_p = 800\, kg/m^3$; $D = 50\ \mu m$; $\alpha = 0.1$;

$L = 0.3048\, m$; $Ec = 0.1$; $\mu = 1.5415 \times 10^{-5}\ kg/m\, sec$.

The primary aim of this study is to investigate the influence of the volume fraction (φ) and Prandtl number (Pr) on the flow dynamics and heat transfer processes involving suspended particulate matter. A numerical solution is obtained using a computational algorithm that employs a non-uniform grid, and the scheme was implemented in MATLAB (Shampine and Kierzenka [34]). The numerical outcomes are examined in the form of graphs for various values of φ and Pr. The heat transfer rate, expressed as the Nusselt number (Nu), and the shear stress, represented by the skin friction coefficient (C_f), are calculated due to their physical relevance.

A specific limiting case of the present model has been validated by comparing the numerical values of the Nusselt number with those reported by Mishra et al. [15], as summarized in Table 1. An excellent agreement is observed over the entire range of Prandtl numbers considered. The absolute differences between the two sets of results are of the order of 10^{-5}, while the corresponding relative errors remain well below 0.005%, indicating negligible numerical deviation. For instance, at $Pr = 0.72$ and $Pr = 1.0$, the relative errors are approximately 0.0009% and 0.0038%, respectively, whereas even at higher Prandtl numbers such as $Pr = 10.0$, the discrepancy remains extremely small. This consistently minimal error confirms the numerical stability, accuracy, and convergence of the present computational scheme. Moreover, the close match across both low and high Prandtl number regimes demonstrates that the present formulation reliably captures the underlying heat transfer physics without introducing spurious numerical artifacts. Hence, the error analysis strongly substantiates the correctness of the numerical implementation and establishes the present results as a trustworthy extension of the existing literature.

The accuracy of the present numerical results is further illustrated through the graphical representation of Table 1, as shown in Fig. 4. The near-perfect overlap between the present results and those reported by Mishra et al. [15] in the figure clearly confirms the precision, consistency, and reliability of the numerical methodology adopted in this study.

Table 1. Comparison of numerical results for Nu

Pr	Nu (Mishra et al. [15])	Nu (Present results)
0.72	1.0884	1.08841
1.0	1.3333	1.33335
3.0	2.5097	2.50976
10.0	4.7969	4.79693

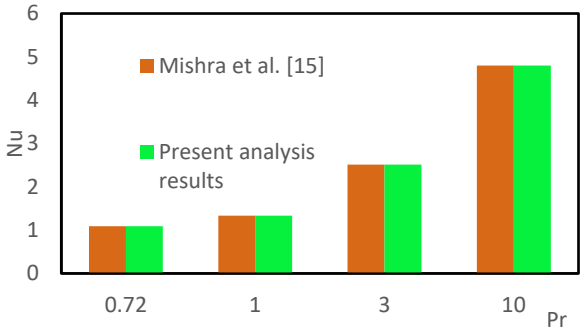

Figure 4. Graphical comparison of present analysis with Mishra et al. [15]

It is important to emphasize that Figures 5-12 display the numerical results for velocity and temperature profiles, which closely resemble those reported in previously published studies on natural convective flows. This similarity serves to validate the accuracy of the numerical findings presented in this investigation.

The velocity and temperature fields for different φ are depicted in Fig 5-8. Figures 5 and 6 illustrate that as the concentration of particles per unit volume in the mixture rises, the velocities of both the carrier fluid and the particle phase decrease.

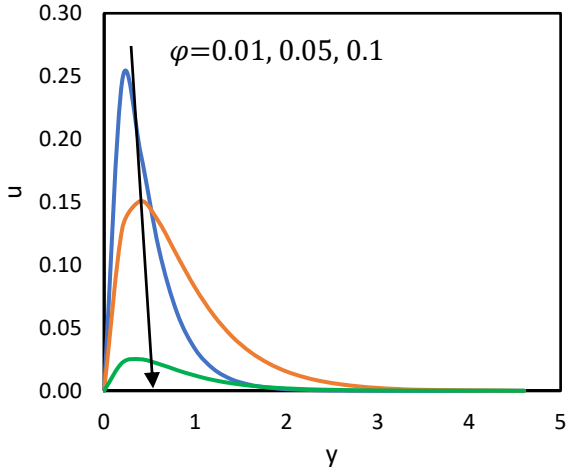

Figure 5. Variation of u with φ

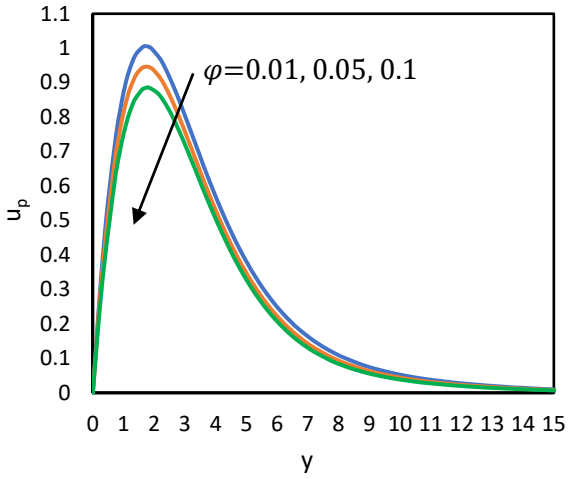

Figure 6. Variation of u_p with φ

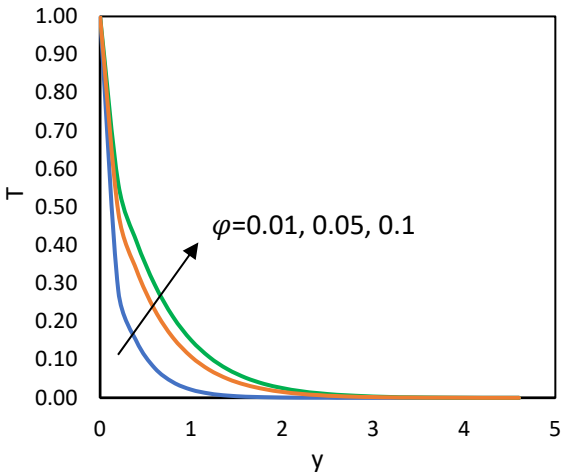

Figure 7. Variation of T with φ

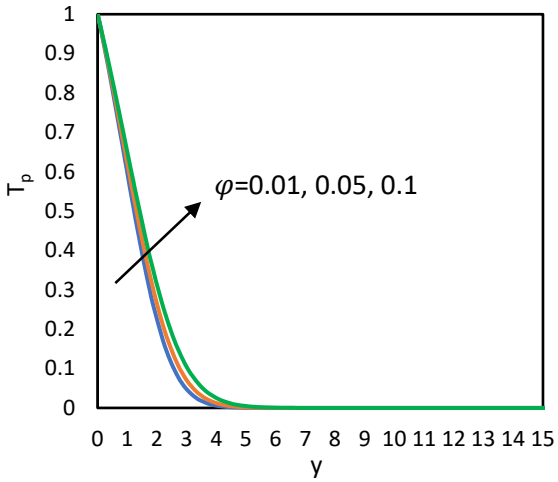

Figure 8. Variation of T_p with φ

In contrast, Figures 7 and 8 indicate that a higher particle concentration results in an increase in the temperatures of both the carrier fluid and particle phases. Additionally, the boundary layer thickness for the particle phase is greater than that of the carrier fluid in both the velocity and temperature distributions. The variation in velocity and temperature

distribution for different values of Pr with respect to y is illustrated in Figures 9 to 12. An increase in Pr values does not influence the velocity of the carrier fluid; however, it leads to an increase in the velocity of the particle phase, as shown in Figures 9 and 10. It is observed that as the Pr value increases, the temperature of the carrier fluid decreases, while the particle phase temperature rises. The rise in Pr results in a reduction in the carrier fluid's temperature distribution. This occurs because lower Pr values correspond to higher thermal conductivity, allowing heat to diffuse more rapidly away from the heated surface compared to higher Prandtl numbers. Consequently, the temperature decreases more quickly for water than for air as the carrier fluid. Moreover, the boundary layer thickness of the particle phase is greater than that of the carrier fluid in terms of both velocity and temperature distributions.

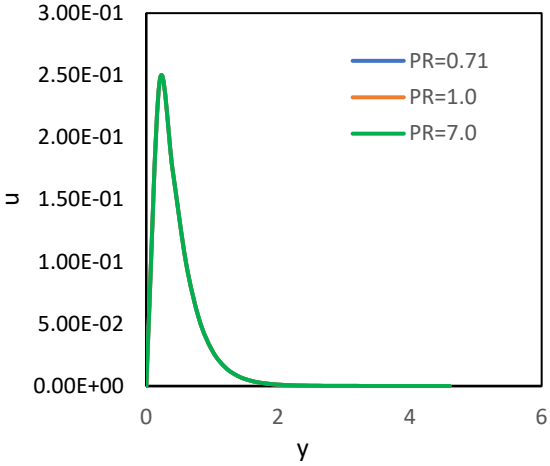

Figure 9. Variation of u with Pr

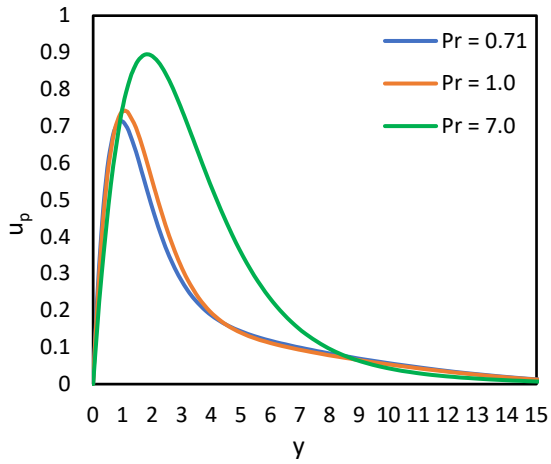

Figure 10. Variation of u_p with Pr

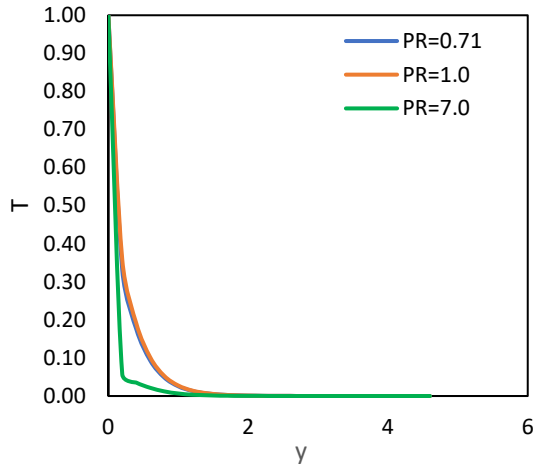

Figure 11. Variation of T with Pr

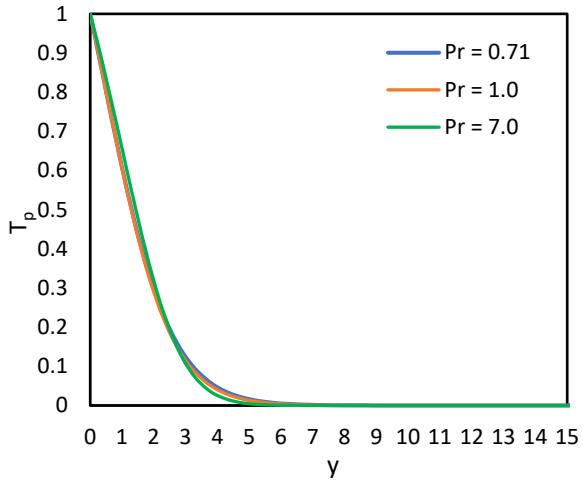

Figure 12. Variation of T_p with Pr

Figure 13 illustrates the streamline patterns of the flow field generated from the velocity components u and v, with color contours representing the magnitude of the velocity field, in the presence of suspended particulate matter for two different Prandtl numbers, namely (a) $Pr = 0.71$ and (b) $Pr = 7.0$, thereby highlighting the influence of thermal diffusivity on the flow structure and momentum transport.

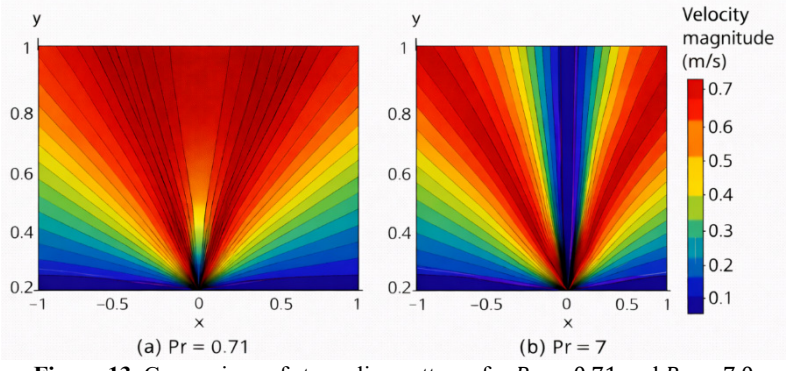

Figure 13. Comparison of streamline patterns for $Pr = 0.71$ and $Pr = 7.0$

For $Pr = 0.71$, which is characteristic of air, the streamlines are relatively more dispersed and smoothly distributed throughout the flow domain. This behavior indicates that thermal diffusion is moderately dominant compared to momentum diffusion, allowing heat to spread efficiently across the fluid. Consequently, the temperature gradients are weaker, resulting in a reduced coupling between the thermal and velocity fields. This leads to broader streamline spacing, gentler curvature, and a less pronounced flow acceleration in the central region, as evidenced by the gradual colour transitions. In contrast, when the Prandtl number is increased to $Pr = 7.0$, corresponding to fluids such as water, the streamline patterns become significantly denser and more concentrated toward the central vertical region. The higher Prandtl number signifies lower thermal diffusivity relative to momentum diffusivity, causing heat to be confined within a thinner thermal boundary layer. This confinement enhances the temperature gradients near the surface, which strengthens buoyancy-induced forces and intensifies the flow circulation. As a result, the streamlines exhibit sharper curvature and closer spacing, particularly near the core region, indicating higher velocity magnitudes and stronger shear effects. The colour contours further corroborate this trend by displaying steeper gradients and elevated peak values compared to the $Pr = 0.71$ case.

The combined influence of φ and Pr on C_f and Nu is illustrated in Figures 14 and 15, respectively. As shown in Figure 14, C_f decreases as the volume fraction (φ) increases across different values of Pr. Conversely, for varying values of φ, the skin friction coefficient C_f exhibits an upward trend with increasing Prandtl number (Pr). This indicates that the highest skin friction is observed when lower values of the volume fraction parameter are combined with higher values of the Prandtl number. This finding underscores the crucial role that the Prandtl number plays in shaping the behavior of skin friction. The interaction between these parameters reveals a complex relationship, where the Prandtl number's influence becomes increasingly dominant, emphasizing its importance in understanding and predicting skin friction coefficient.

Similarly, Figure 15 demonstrates that the Nu values diminish with an increase in φ across various Pr values. In contrast, for different φ values, the Nusselt number (Nu) tends to increase with rising Prandtl numbers. The findings indicate that the highest heat transfer coefficient is achieved when the volume fraction parameter is maintained at relatively lower values, while the Prandtl number is elevated to higher levels. This observation underscores the pivotal role of the Prandtl number in governing heat transfer dynamics, emphasizing its substantial impact on the efficiency and behavior of heat transfer processes.

At a fixed Prandtl number ($Pr \approx 3$), increasing the particle volume fraction from $\varphi = 0.01$ to 0.10 leads to a reduction in C_f from approximately 1.12 to 1.07, corresponding to a decrease of about 4-5%. A similar suppressing trend is observed for heat transfer, where Nu decreases from nearly 0.41 to 0.385, indicating an approximate 6% reduction. This behavior is attributed to enhanced effective viscosity and particle–fluid interactions, which thicken the momentum and thermal boundary layers and weaken wall gradients. In contrast, at a fixed particle volume fraction ($\varphi \approx 0.05$), increasing the Prandtl number from 0.7 to 7 enhances the skin friction coefficient by nearly 6-7% and the Nusselt number by about 10%. Higher Prandtl numbers reduce thermal diffusivity, resulting in a thinner thermal boundary layer and steeper temperature gradients at the wall, thereby intensifying heat transfer. Overall, particle loading tends to suppress transport processes, whereas increasing the Prandtl number significantly improves thermal performance in buoyancy-driven two-phase flows with suspended particulate matter. The boundary layer thickness is set to an optimized value of 15.0 to ensure accurate and reliable numerical results.

These observations indicate a complex interaction between φ and Pr, highlighting their significant roles in influencing both heat transfer and skin friction characteristics in the flow system.

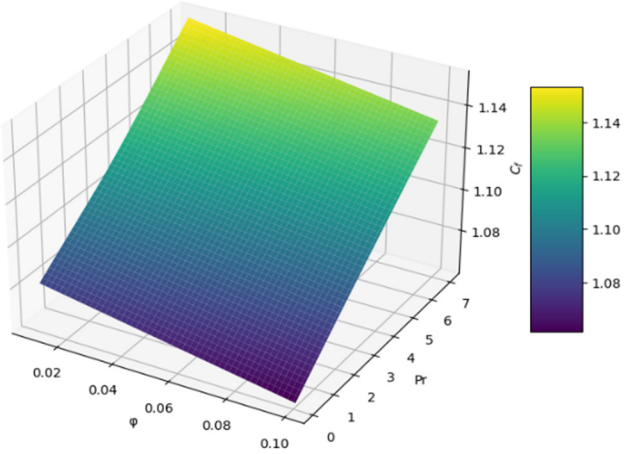

Figure 14. Combined effects of φ and Pr on skin friction coefficient

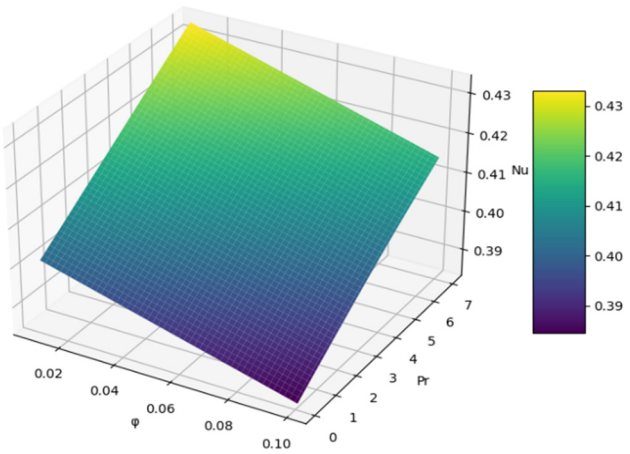

Figure 15. Combined effects of φ and Pr on Nusselt number

5. CONCLUSIONS

This study examines the impact of volume fraction parameter (φ) and Prandtl number (Pr) on the boundary layer properties, skin friction, and heat transfer in a steady, laminar, incompressible natural convective two-phase flow past a vertical plate with suspended particles. The key results are outlined below:

i. The volume fraction decreases the velocities of both the particle phase and carrier fluid, but it increases the temperatures of both the carrier fluid and particle phase within the boundary layer region.

ii. Pr has no significant impact on the velocity of the carrier fluid; however, it enhances the velocity of the particle phase within the boundary layer region.

iii. Pr leads to a reduction in the temperature of the carrier fluid while simultaneously raising the temperature of the particle phase within the boundary layer region.

iv. An increase in φ results in a decrease in both the Nusselt number and the skin friction coefficient. Conversely, a rise in Pr enhances both the Nusselt number and the skin friction coefficient.

v. Since the Prandtl number is 6.2 for pure water and 0.71 for air, heat transfer occurs at a much higher rate in fluids like pure water than in air.

vi. An increase in the Prandtl number enhances the rate of heat transfer from the plate surface to the surrounding fluid. This improvement, influenced by the Prandtl number effect, promotes more efficient heat dissipation into the cooler fluid, thereby aiding in the cooling of the plate. The enhanced thermal performance of fluids containing suspended particles, driven by this effect, proves particularly beneficial in manufacturing processes involving plane wall-shaped products, which are prone to high temperatures during production. By improving heat transfer efficiency, the Prandtl number effect supports better temperature regulation, leading to reduced product temperatures, improved manufacturing efficiency, and enhanced product quality.

This study demonstrates that the volume fraction is a key factor in diminishing both resistance and the efficiency of heat transfer within a system. In contrast, the Prandtl number exerts a positive effect on fluid flow properties and enhances thermal performance. A higher Prandtl number typically indicates that momentum diffusivity is lower compared to thermal diffusivity, resulting in a thinner thermal boundary layer. This leads to improved thermal gradients and more efficient heat exchange. Gaining a comprehensive understanding of these relationships is essential for the effective optimization of heat transfer processes in various engineering applications like metal casting, glass production, and chemical processing, where maintaining optimal thermal conditions ensures product quality, process stability, and energy efficiency. By optimizing heat transfer characteristics through control of the Prandtl number, industries can achieve better thermal management, reduce energy consumption, and improve the overall performance of thermal systems.

ORCID

Sasanka Sekhar Bishoyi, https://orcid.org/0000-0003-0760-9460; **Sakambari Mishra,** https://orcid.org/0009-0007-9088-7571
Aditya Kumar Pati, https://orcid.org/0000-0003-0966-5773; **Prasanta Kumar Rath,** https://orcid.org/0000-0002-3869-9705

REFERENCES

[1] M.A. Arabi, and B. Sakr, "Natural convection heat transfer from inclined isothermal plates", International J. Heat Mass Transfer," **31**(3), 559-565 (1988). https://doi.org/10.1016/0017-9310(88)90037-3

[2] W. Lin, S.W. Armfield, and P.L. Morgan, "Unsteady natural convection boundary-layer flow along a vertical isothermal plate in a linearly stratified fluid with Pr>1," International J. Heat Mass Transfer, **45**, 451-459 (2002). https://doi.org/10.1016/s0017-9310(01)00154-5

[3] F. Kimura, K. Kitumara, M. Yamaguchi, and T. Asami, "Fluid flow and heat transfer of natural convection adjacent to upward-facing inclined heated plates," Heat Transfer-Japanese Research, **32**(3), 278-291 (2003). https://doi.org/10.1002/htj.10091

[4] S. Siddiqa, M.A. Hossain, and S.C. Saha, "Two-phase natural convection flow of a dusty fluid," International Journal of Numerical Methods for Heat & Fluid Flow, **25**(7), 1542-1556 (2015). https://doi.org/10.1108/hff-09-2014-0278

[5] H. Gasmi, U. Khan, A. Zaib, A. Ishak, S.M. Eldin, and Z. Raizah, "Analysis of mixed convection on two-phase nanofluid flow past a vertical plate in Brinkman-extended Darcy porous medium with Nield conditions," Mathematics, **10**(20), 3918 (2022).

[6] A. Kitagawa, R. Kobayashi, P. Denissenko, and Y. Murai, "Natural convection heat transfer enhancement using bubble injection between vertical parallel plates," International Journal of Heat and Mass Transfer, **202**, 123658 (2023). https://doi.org/10.1016/j.ijheatmasstransfer.2022.123658

[7] D. Khan, G. Ali, P. Kumam, M.Y. Almusawa, and A.M. Galal, "Time fractional model of free convection flow and dusty two-phase couple stress fluid along vertical plates," ZAMM-Journal of Applied Mathematics and Mechanics/Zeitschrift für Angewandte Mathematik und Mechanik, **103**(5), e202200369 (2023). https://doi.org/10.1002/zamm.202200369

[8] A.M. Obalalu, M.O. Oni, U. Khan, A. Abbas, T. Muhammad, and A. Zaib, "Two-phase numerical simulation for the heat and mass transfer evaluation across a vertical deformable sheet with significant impact of solar radiation and heat source/sink," Arabian Journal for Science and Engineering, **49**(8), 11053-11071 (2024). https://doi.org/10.1007/s13369-023-08585-z

[9] R.H. Hameed, Q.R. Al-Amir, H.K. Hamzah, F.H. Ali, and A. Alahmer, "Enhancing Natural Convection Heat Transfer Through Dome-Shaped Nanofluid Enclosures: Two-Phase Simulation Analysis," Heat Transfer Engineering, **46**(15), 1331-1356 (2024). https://doi.org/10.1080/01457632.2024.2378562

[10] M. Shi, Z. Duan, X. Zhao, Z. Wang, S. Liu, and H. Xue, "Experimental investigation on two-phase flow instability induced by direct contact condensation in open natural circulation," Energy, **292**, 130547 (2024). https://doi.org/10.1016/j.energy.2024.130547

[11] S. Akter, A. Hossain, M.M. Islam, and M.M. Molla, "Finite difference simulation of natural convection of two-phase hybrid nanofluid along a vertical heated wavy surface," Journal of Taibah University for Science, **18**(1), 2358548 (2024). https://doi.org/10.1080/16583655.2024.2358548
[12] N.H. Zamri, A.R.M. Kasim, M.H. Hassan, T.L. Hassan, S.M. Zokri, N.S. Arifin, and A.A. Taofeeq, "Theoretical Analysis of Two-Phase Mixed Convection Flow: Effects of Fluid-particle Interaction and Mass Concentration on Velocity, Temperature and Skin Friction. Journal of Advanced Research in Computing and Applications, **38**(1), 23-38 (2025). https://doi.org/10.37934/arca.38.1.2338
[13] S.L. Soo, *Fluid Dynamics of Multiphase Systems*, (Blaisdell Publishing co., Waltham MA, 1967)
[14] P.K. Tripathy, T. Samantara, and S. Kanungo, "Radiation effect on convective boundary layer dusty flow over a stretching surface," AIP Advances, **14**(3), 035151 (2024). https://doi.org/10.1063/5.0188957
[15] J. Mishra, T. Samantara, and P.K. Tripathy, "Effects of Electrification and Transverse Force on Dusty Flow over a Linear Stretching Sheet," CFD Letters, **16**(2), 151-161 (2024). https://doi.org/10.37934/cfdl.16.2.151161
[16] S.J. Li, L.T. Zhu, X.B. Zhang, and Z.H. Luo, "Recent advances in CFD simulations of multiphase flow processes with phase change," Industrial & Engineering Chemistry Research, **62**(28), 10729-10786 (2023). https://doi.org/10.1021/acs.iecr.3c00706
[17] X. Wu, J. Huang, Y. Zhuang, Y. Liu, J. Yang, H. Ouyang, and X. Han, "Prediction Models of Saturated Vapor Pressure, Saturated Density, Surface Tension, Viscosity and Thermal Conductivity of Electronic Fluoride Liquids in Two-Phase Liquid Immersion Cooling Systems: A Comprehensive Review," Applied Sciences, **13**(7), 4200 (2023). https://doi.org/10.3390/app13074200
[18] P. Barnoon, D. Toghraie, and S. Rostami, "Optimization of heating-cooling generators with porous components/cryogenic conductors on natural convection in a porous enclosure: Using different two-phase models and single-phase model and using different designs," International Communications in Heat and Mass Transfer, **111**, 104472 (2020). https://doi.org/10.1016/j.icheatmasstransfer.2019.104472
[19] S. Alapati, "Simulation of natural convection in a concentric hexagonal annulus using the lattice Boltzmann method combined with the smoothed profile method," Mathematics, **8**(6), 1043 (2020). https://doi.org/10.3390/math8061043
[20] O.R. Alomar, R.R. Mohammed, M.A. Mendes, S. Ray, and D. Trimis, "Numerical investigation of two-phase flow in anisotropic porous evaporator," International Journal of Thermal Sciences, **135**, 1-16 (2019). https://doi.org/10.1016/j.ijthermalsci.2018.08.026
[21] O.R. Alomar, "Analysis of variable porosity, thermal dispersion, and local thermal non-equilibrium on two-phase flow inside porous media," Applied Thermal Engineering, **154**, 263-283 (2019). https://doi.org/10.1016/j.applthermaleng.2019.03.069
[22] O.R. Alomar, M.A. Mendes, D. Trimis, and S. Ray, "Numerical simulation of complete liquid–vapour phase change process inside porous media: A comparison between local thermal equilibrium and non-equilibrium models," International journal of thermal sciences, **112**, 222-241 (2017). https://doi.org/10.1016/j.ijthermalsci.2016.09.014
[23] A.K. Rauta, "Modelling of two-phase flow over a stretching sheet with analysis of boundary layer flow and heat transfer characteristics," International Journal of Mathematics Trends and Technology-IJMTT, 41 (2017). https://doi.org/10.14445/22315373/ijmtt-v41p519
[24] A.K. Pati, and P. Jena, "Optimizing thermal performance of chemically reactive and thermally radiative nanofluid flow with convective heating and triboelectric effect of nanoparticles," Multiscale and Multidisciplinary Modeling, Experiments and Design, **8**(7), 336 (2025). https://doi.org/10.1007/s41939-025-00923-y
[25] A.K. Pati, A. Misra, and S.K. Mishra, "Thermal analysis of Ag-water nanofluid flow induced by a horizontally stretching cylinder with electrified nanoparticles," Sigma Journal of Engineering & Natural Sciences, **43**(4), (2025). https://doi.org/10.14744/sigma.2025.00111
[26] A.K. Pati, A. Misra, and S.K. Mishra, "Heat and mass transfer analysis on natural convective boundary layer flow of a Cu-water nanofluid past a vertical Flat plate with electrification of nanoparticles," Advances and Applications in Fluid Mechanics, **23**(1), 1-15 (2019). https://doi.org/10.17654/fm023010001
[27] S.S. Bishoyi, A.K. Pati, S. Mishra, A. Misra, and S.K. Mishra, "Lie group analysis of triboelectric nanoparticle influence on heat and mass transfer in buoyancy-driven nanofluid flow with multiple slip effects," Journal of Electrostatics, **139**, 104220 (2026). https://doi.org/10.1016/j.elstat.2025.104220
[28] A.K. Pati, A. Misra, and S.K. Mishra, "Effect of electrification of nanoparticles on natural convective boundary layer flow and heat transfer of a Cu-Water nanofluid past a vertical flat plate," International Journal of Engineering, Science and Mathematics, **6**(8), 1254-1264 (2017).
[29] S. Mishra, A.K. Pati, A. Misra, and S.K. Mishra, "Thermal performance of nanofluid flow along an isothermal vertical plate with velocity, thermal, and concentration slip boundary conditions employing Buongiorno's revised non-homogeneous model," East European Journal of Physics, (4), 98-106(2024). https://doi.org/10.26565/2312-4334-2024-4-09
[30] A.K. Pati, M.M. Rout, R. Sahu, I.S. Ramakoti, K.K. Panda, and K.C. Sethi, "Chemical reaction, electrification, Brownian motion and thermophoresis effects of copper nanoparticles on nanofluid flow with skin friction, heat and mass transfer," East European Journal of Physics, (4), 152-158 (2024). https://doi.org/10.26565/2312-4334-2024-4-14
[31] B. Otterman, "Particle migrations in laminar mixing of a suspension with a clear fluid", ZAMP, 20, 730-749 (1969). https://doi.org/10.1007/bf01590631
[32] A. Misra, S.K. Mishra, and J. Prakash, "Modeling electrification of suspended particulate matter (SPM) in a two-phase laminar boundary layer flow and heat transfer over a semi-infinite flat plate," Int. Commun. Heat Mass Transf. **38**(8), 1110-1118 (2011). https://doi.org/10.1016/j.icheatmasstransfer.2011.05.015
[33] S.K. Mishra and P.K. Tripathy, "Mathematical and Numerical modeling of two-phase flow and heat transfer using non-uniform grid", Far East journal of Applied Mathematics, **54**(2), 107-126 (2011).
[34] L.F. Shampine, and J. Kierzenka, "A BVP Solver based on residual control and the MATLAB PSE," ACM Trans. Math. Softw. **27**(3), 299-316 (2001). https://doi.org/10.1145/502800.502801

АНАЛІЗ МЕТОДОМ СКІНЧЕННИХ РІЗНИЦЬ ВПЛИВУ ЧИСЛА ПРАНДТЛЯ ТА ОБ'ЄМНОЇ ЧАСТКИ ЧАСТИНОК НА ТЕРТЯ ПО ПОВЕРХНІ ТА ПЕРЕНОС ТЕПЛА У ДВОФАЗНОМУ ПОТОЦІ, ОБУМОВЛЕНОМУ ПЛАВУЧІСТЮ, ЗІ ЗВАЖЕНИМИ ЧАСТИНКАМИ (SPM)

Сасанка Сехар Бішоїї[1], Сакамбарі Мішра[2], Адітья Кумар Паті[3]*, Прасанта Кумар Рат[3]

[1]Університет NIST, Берхампур, Ганджам, Одіша, Індія

2Коледж фундаментальних наук та гуманітарних наук, Університет сільського господарства та технологій Одіші, Бхубанешвар, Одіша, Індія

[3]Університет технологій та менеджменту Центуріон, Паралакхемунді, Одіша, Індія

Було проведено числове дослідження нестисливого, ламінарного двофазного потоку, що залежать від плавучості, що містить зважені частинки навколо вертикальної пластини. Незважаючи на актуальність таких систем, попередні дослідження значною мірою ігнорували природні конвекційні двофазні потоки з твердими частинками, особливо щодо ролі таких параметрів, як число Прандтля та об'ємна частка. Заповнення цієї прогалини в дослідженнях є критично важливим, оскільки ці параметри суттєво впливають на поведінку потоку та теплопередачу, які є життєво важливими в екологічних, промислових та теплових застосуваннях. Це дослідження зосереджено на вивченні впливу об'ємної частки та числа Прандтля на характеристики двофазного потоку за допомогою неявного методу скінченних різниць, застосованого до неоднорідної сітки. Аналіз оцінює поведінку прикордонного шару, швидкість теплопередачі та коефіцієнти тертя поверхневого шару. Картини ліній струму проілюстровано для різних значень числа Прандтля, тоді як контурні топології представлені для демонстрації комбінованого впливу числа Прандтля та об'ємної частки на тертя поверхневого шару та швидкість теплопередачі. Результати показують, що збільшення об'ємної частки зменшує як число Нуссельта, так і коефіцієнт тертя поверхневого шару, тоді як вище число Прандтля посилює обидва. Покращена теплова реакція, що спостерігається при вищих числах Прандтля, особливо корисна у виробничих процесах, що включають плоскі стінкоподібні структури, схильні до термічних напружень. Ці висновки мають практичне значення для проектування та оптимізації теплообмінників, систем змащення та рішень для терморегулювання в електронних пристроях.

Ключові слова: *теплопередача; потік, зумовлений плавучістю; число Прандтля; об'ємна частка частинок; зважені тверді частинки; неявний метод скінченних різниць*